Predicting flux in Discrete Fracture Networks via Graph Informed Neural Networks

https://doi.org/10.3311/PPme.38444

Periodica Polytechnica Mechanical Engineering

Friction Stir Welding of Laser-powder Bed Fusion Manufactured A20X

Mohammad Abankar[1,2*], Vincenzo Lunetto[1,2], Manuela De Maddis[1,2], Franco Lombardi[1,2], Valentino Razza[1,2], Pasquale Russo Spena[1,2]

[1] Department of Management and Production Engineering, Politecnico di Torino, Corso Duca degli Abruzzi 24, 10129 Turin, Italy
[2] Advanced Joining Technologies Laboratory (J-Tech@PoliTO), Politecnico di Torino, Corso Duca degli Abruzzi 24, 10129 Turin, Italy
* Corresponding author, e-mail: mohammad.abankar@polito.it

Received: 30 September 2024, Accepted: 27 October 2024, Published online: 31 October 2024

Abstract

This study investigates butt friction stir welding of 4 mm thick A20X plates, which were produced using additive manufacturing through laser-powder bed fusion. The plates were joined at varying process parameters, including different welding and rotational speeds. Both the microstructure and the mechanical strength of the joints were examined, comparing joints in both as-printed and as-welded conditions.

The joints welded at a welding speed of 100 mm/min and a rotational speed of 1500 rpm exhibited superior mechanical properties compared to those produced with other parameter settings. The results show that decreasing the rotational speed while increasing the welding speed leads to the formation of tunnel defects, compromising joint integrity and resulting in lower ultimate tensile strength. In contrast, the combination of 100 mm/min welding speed and 1500 rpm rotational speed produced defect-free joints, with an average ultimate tensile strength of 335 MPa and an elongation at fracture of 8.5%.

Keywords

A20X alloy, additive manufacturing, FSW, mechanical properties, microstructure

1 Introduction

Aluminum alloys stand out in lightweight engineering applications for their excellent specific strength and toughness [1]. In this regard, additively manufactured A20X alloy is a newly advanced high-strength alloy in the 2xxx series, developed by Aeromet International [1, 2]. This alloy contains boron and titanium elements that favor the formation of an ultrafine-grained aluminum matrix with a micrometric grain size (around 1 μm) [3–5]. Such fine microstructures result from the strong precipitation of very fine TiB_2 and Al_2Cu second phases within a homogeneous and texture-free α-aluminum matrix. Ti and B do not tend to react with aluminum, so no brittle second phases form at the interface of the Al matrix and TiB_2 particles [5]. The outstanding strength of A20X is further improved by θ- and Ω-Al_2Cu precipitates [1]. Yield strength falls within the range of 300–330 MPa for most laser powder bed fusion (L-PBF) A20X alloys [1, 6–8].

The high dislocation density around the heterogeneously distributed nano-sized TiB_2 particles provides suitable sites for the precipitation of Al_2Cu during aging heat treatment. A supersaturated solid solution (SSSS) forms after a solubilization treatment, while subsequent aging generates at first Guinier-Preston (GP) zones and, then, the formation of θ-Al_2Cu precipitates from the transition from metastable to stable phases, as in [3]:

$$\begin{aligned}&\text{GP zones} \rightarrow \text{metastable } \theta'' \rightarrow \text{metastable } \theta' \\ &\rightarrow \text{stable } \theta - Al_2Cu \text{ precipitates}\end{aligned} \quad (1)$$

Ω-Al_2Cu precipitates, instead, form during T7 heat treatment (solubilization treatment and overaging) through the following phase transformations [1]:

$$SSSS \rightarrow Mg - Ag \text{ co} - \text{clusters} \rightarrow \Omega - Al_2Cu \quad (2)$$

The A20X alloy mainly features two distinct precipitates: plate-like Ω on the {111} and θ'/ θ'' precipitates on the {001} aluminum habit planes [9]. Avateffazeli et al. [1] attributed the primary strengthening mechanisms improving the mechanical strength of A20X to several factors, including TiB_2 particles, solute atoms, small grain size, and residual stresses. TiB_2 particles transfer the external load from the matrix to hard TiB_2/matrix interfaces.

Cite this article as: Abankar, M., Lunetto, V., De Maddis, M., Lombardi, F., Razza, V., Russo Spena, P. "Friction Stir Welding of Laser-powder Bed Fusion Manufactured A20X", Periodica Polytechnica Mechanical Engineering, 2024. https://doi.org/10.3311/PPme.38444

Solute atoms of Mg and Ag increase strength through local distortions of the Al crystal lattice. Moreover, they also promote the formation of Ag-Mg co-clusters serving as nucleation sites for Ω-Al_2Cu precipitation. Other solute atoms, like Ti and Cu, further increase strength through solid solution strengthening [10]. According to the Hall-Petch relationship [11], finer grain size increases the strength of any polycrystalline metal. During the solidification process and subsequent cooling phase, the significant difference between the coefficient of thermal expansion between the Al-matrix and TiB_2 particles increases the dislocation density around the TiB_2/matrix interface and leads to the formation of residual stresses [5].

Currently, no studies have addressed the welding of A20X alloy or the influence of different joining processes on weld quality. Friction stir welding (FSW) offers a promising solution for joining this advanced alloy, as it overcomes many limitations of traditional fusion welding methods. Operating under solid-state, FSW minimizes the heat-affected zone, residual stresses, and thermal distortions. This study investigates the effects of FSW on the mechanical and microstructural properties of additively manufactured A20X produced via laser power bed fusion (L-PBF) at varying welding parameters, including different rotation and welding speeds. The research also aims to identify the optimal process parameters for obtaining joints with superior mechanical properties in terms of hardness and strength.

2 Materials and methods

A20X plates (4 mm · 75 mm · 55 mm) were produced via L-PBF technology. Their chemical composition is reported in Table 1, based on the supplier technical datasheet. The metal printing parameters were laser power of 370 W, powder size distribution range from 20 to 63 μm, hatch spacing of 45−55 μm, and layer thickness of 30 μm. The average density of the plates was 99.7%. All samples had their length parallel to the build direction.

The following process parameters were used during the FSW process of A20X: plunge depth of 4 mm, plunge speed of 10 mm/min, 2° tilt angle of the tool, and dwell time of 2 s. Welding speed was varied from 100 to 500 mm/min, while rotational speed was from 900 to 1500 rpm to obtain two distinct welding conditions with either the highest or lowest heat input involved: 100 mm/min − 1500 rpm, and 500 mm/min − 900 rpm, respectively. For clarity, samples were labeled as Vx-wy, where "V" stands for welding speed, "w" rotational speed, "x" and "y" are the corresponding numerical values. As a result, the two welding conditions have been labeled as V100-w1500 and V500-w900. The FSW campaign was performed using an FSW machine (mod. FSW100 from Stirtec GmbH) available at the interdepartmental research center on advanced joining technologies - J-Tech@PoliTO - of the Politecnico di Torino, Fig. 1(a). The FSW tool was made of S705 high-speed steel (alloyed with Co, Mo, Cr, V, and W) in quenching and tempering condition, and hardness of 65 HRC, Fig. 1(b). The tool had a 12 mm flat scrolled shoulder to promote metal stirring. The width of the spiral groove on the scrolled shoulder was 0.4 mm and a depth of 0.2 mm. The shoulder ends with a 4 mm truncated conical pin featuring a threaded surface and a cone angle of 15°. An argon shielding gas was flown, with a flow rate of 10 l/min, through two nozzles positioned 2 cm from the rear and front of the FSW tool to protect the weld from oxidation.

The mechanical properties of the FSW joints, including ultimate tensile strength (UTS), yield strength (YS), and elongation at fracture, were assessed through tensile tests according to EN ISO 6892-1:2016 standard [12] with a Zwick/Roell mod. Z050 tensile tester machine at a crosshead speed of 10 mm/min. As shown in Fig. 2, these samples were extracted from each weld using wire electrical discharge machining with a geometry based on the DIN 50125 standard [13]. The cross-sections of the FSW joints were examined using a Carl Zeiss mod. Axio Vert. A1 optical microscope. The metallographic samples were prepared with a standard procedure including grinding, polishing, and final etching with a Keller's reagent.

The hardness of the as-built and V100-w1500 joints was measured by Vickers hardness measurements. The hardness test was conducted based on the ASTM E92-17 standard [14] using an Innovatest mod. NOVA 130, with a 500 g load, a dwell time of 15 s, and a spacing distance of 1 mm between two successive indentations.

3 Results and discussion

3.1 Microstructure and hardness examinations

In the FSW process, the stirring action of the pin and the friction between the shoulder and the plates are the main factors contributing to the heat input produced within the

Table 1 Chemical composition of A20X plates according to the supplier technical datasheet

Element	*Al*	*Si*	*Mg*	*B*	*Cu*	*Fe*	*Ag*	*Ti*
% wt.	balance	0.1 max	0.2 − 0.33	1.25 − 1.55	4.2 − 5	0.08 max	0.6 − 0.9	3 − 3.85

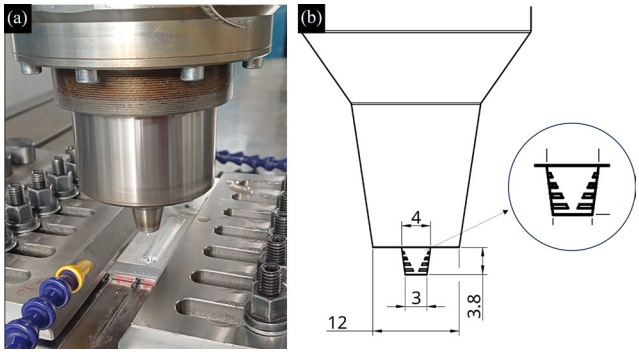

Fig. 1 (a) FSW equipment and (b) tool geometry (in mm) used for the welding tests

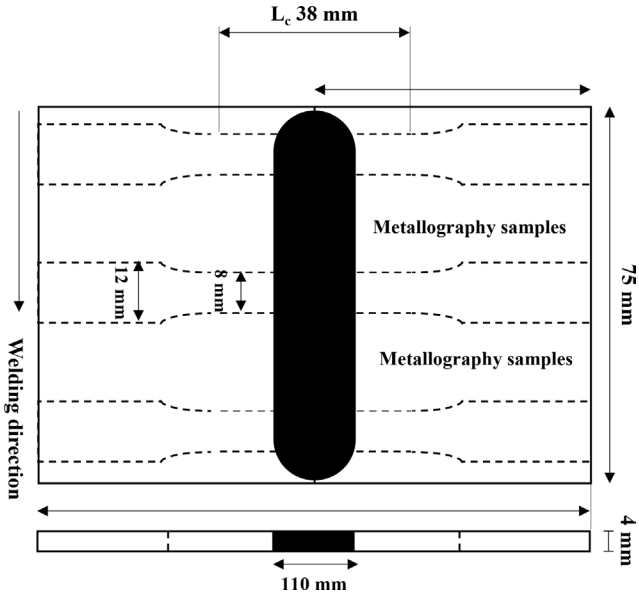

Fig. 2 Sketch of the FSW welds, tensile, and metallographic samples

weld and its surrounding areas [15]. Heat input, defined as the heat energy applied to the workpiece per unit length (J/mm), can be estimated using Eq. (3) [16]:

$$\text{Heat input}\,\frac{J}{mm}=\eta\left(\frac{\omega\cdot T}{v}\right) \tag{3}$$

where T is the tool torque (Nm), η is the efficiency factor (0.9 for aluminum and copper [17]), v is the welding speed (mm/min), and is the tool rotational speed (rpm). The torque during the welding phase for the V100-w1500 and V500-w900 joints was monitored in real-time during the FSW process, with recorded values of 11 Nm and 16 Nm, respectively. Using Eq. (3), the corresponding heat inputs were computed to be 216 J/mm and 26 J/mm for the V100-w1500 and V500-w900 joints. These results are consistent with the higher frictional heat experienced by the V100-w1500 joint, due to its lower welding and higher rotational speeds.

Fig. 3 shows the welds seam of the V100-w1500 and V500-w900 FSW joints. The joint width remains consistent between the two because the same plunge depth and shoulder diameter were used in their welding. A comparison of the joint surfaces reveals that the V100-w1500 joint features a smooth and uniform seam, while increasing the welding speed and decreasing the rotational speed results in a rougher seam surface, with visible imprints from pin revolutions. The optimal weld appearance, characterized by reduced surface roughness, is achieved by lowering the welding speed and increasing the rotational speed. This welding condition leads to higher heat inputs and, hence, to a stronger metal stirring that facilitates smoother weld surfaces [18].

Fig. 4 shows the cross-sections of the V100-w1500 and V500-w900 joints. As well-known, the stir zone (SZ) is asymmetric because of the inhomogeneous material flow between the advancing side (AS) and the retreating side (RS) of the joint. The AS exhibits more pronounced material flow, as evidenced by a clear line between the SZ and the base metal (BM). Onion rings (OR) are also observable in both joints, even though they are less evident in the V100-w1500 joint. In addition, Fig. 4 reveals a tunnel defect in the V500-w900

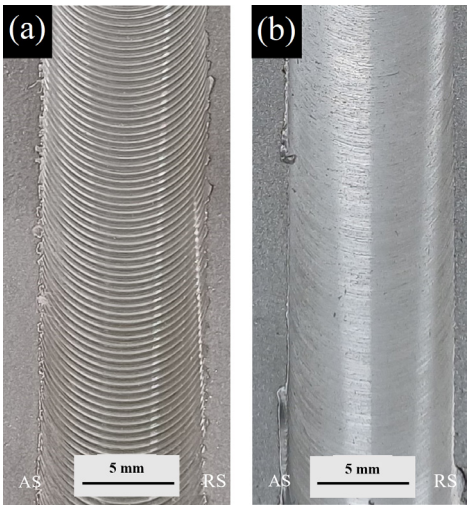

Fig. 3 The visual aspect of the FSW joints: (a) V500-w900, (b) V100-w1500

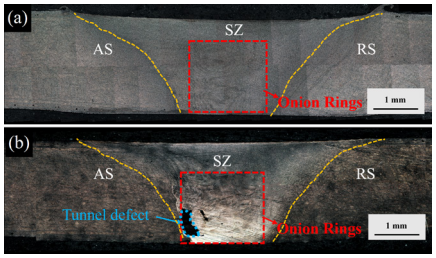

Fig. 4 Cross-section of the FSW joints: (a) V100-w1500, (b) V500-w900

joint, which is absent in the V100-w1500 joint. This defect is attributed to insufficient heat input and metal stirring in the V500-w900 joint. Due to the severity of the tunnel defect, no further analysis was conducted on this sample.

Fig. 5 displays a microstructural comparison between the as-printed A20X and the SZ of the V100-w1500 joint. The BM microstructure, shown in images (a) and (b), reveals a highly densified structure with minimal porosity, a result of the proper additive manufacturing process. Microstructural analysis of both the BM and SZ, depicted in images (c) and (d), shows a fine microstructure in both the as-printed and welded A20X, with grain sizes of 1 μm and 3 μm, respectively. This is in contrast with other AM aluminum alloys, such as AlSi10Mg, which typically exhibit columnar grains [3]. The fine and equiaxed grain structure in A20X is primarily attributed to the presence of TiB_2 particles, which act as effective grain refiners due to their high coherency with the α-aluminum crystal lattice [19]. As a result, A20X maintains a refined grain structure even after welding [20].

Fig. 6 shows the Vickers hardness map of the V100-w1500 FSW joint. The average hardness of the as-printed A20X is 115 ± 5 HV, while the hardness at the top of the SZ reaches 125 ± 3 HV. The SZ underwent a severe plastic deformation followed by dynamic recrystallization (DRX), resulting in notable grain refinement [21].

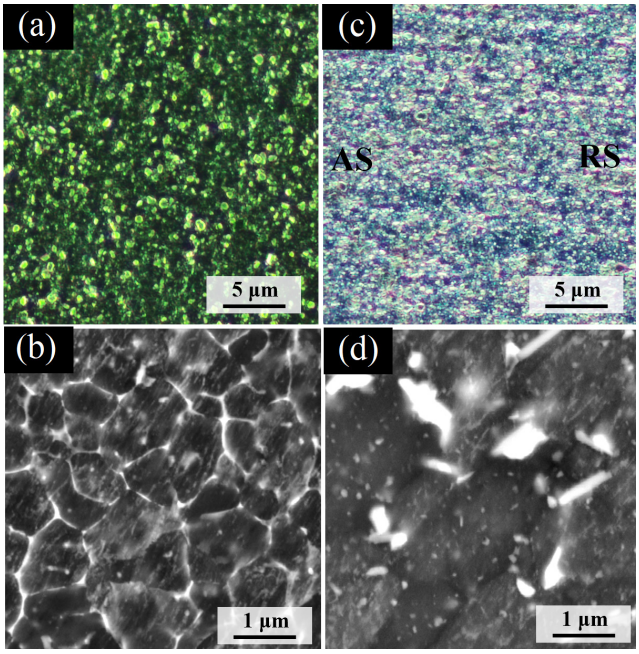

Fig. 5 (a) Optical and (b) SEM images of the as-built microstructure, (c) optical and (d) SEM images of the SZ microstructure of the FSW joints made with 100 mm/min welding speed and 1500 rpm of rotational speed

Previous studies have also reported that the stirring action in FSW can remarkably refine the microstructure in the SZ compared to the BM and HAZ [21, 22]. However, in the case of A20X as-built microstructure, TiB_2 particles act as strong grain refiners, providing nucleation sites for new grains during metal solidification, keeping a fine grain size in the BM. Since there is no significant difference in grain size between the BM and SZ, as observed through the optical and SEM images of Fig. 5, the high heat input achieved during FSW (calculated using Eq. (3)) can induce phase transformations, coarsening, or even full decomposition of metastable precipitates [23–27]. In A20X, this is likely associated with the precipitation of Al2Cu particles, which increase hardness up to 125 ± 3 HV.

3.2 Joint tensile strength

Fig. 7 shows the results of the tensile tests performed on both as-printed and welded A20X plates. The as-printed samples exhibit an average ultimate strength (UTS), yield strength (YS), and elongation at fracture of 384 ± 3 MPa, 284 ± 21 MPa, and 11.5 ± 2 %, respectively. For the V100-w1500 joints, these values were reduced to 335 ± 17 MPa, 269 ± 2, and 8.5 ± 3, respectively. The yield stress was determined using the conventional 0.2 % strain offset method from the stress-strain curve. Moreover, no significant necking (less than 5%) was observed in the fractured samples.

For comparison, Du et al. [28] reported that FSW on AlSi10Mg alloy resulted in a UTS of 240 MPa, a 47%

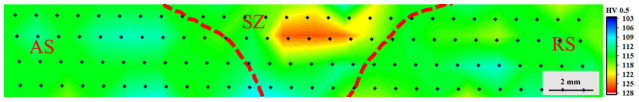

Fig. 6 Vickers hardness map of the FSW joints with welding speed of 500 mm/min and rotational speed of 1500 rpm

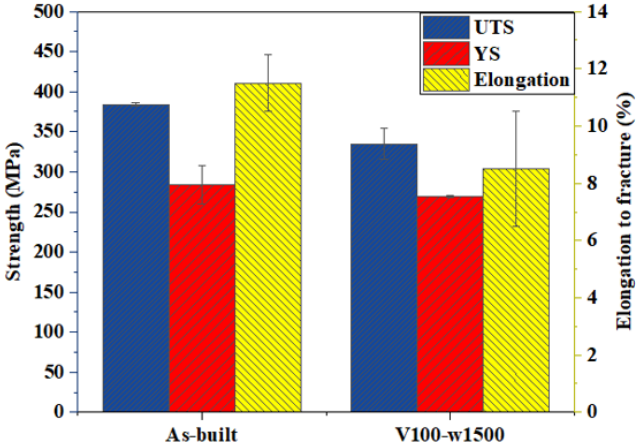

Fig. 7 Tensile results for the as-printed and A20X FSW joints

decrease from the as-built value of 451 MPa. Similarly, Moeini et al. [29] found that FSW of AlSi12 plates led to a 33% reduction in UTS, dropping from 450 to 300 MPa compared to the as-built samples. In this study, the A20X joint only experienced a 13% reduction in UTS relative to the as-built condition, indicating the effectiveness of FSW in preserving the mechanical properties of this additively manufactured aluminum alloy.

4 Conclusions

This study investigates the microstructural and mechanical properties of friction stir welded joints of laser powder bed fusion additively manufactured A20X, assessing the feasibility and influence of solid-state technology on joint strength and quality. The main results are summarized as follows:

- the stir zone exhibits a very fine grain size structure like the base material because of the dynamic recrystallization caused by the stirring action during the joining process;
- the heat input developed during welding increases the hardness of the welded joints to 125 HV, compared to 115 HV in the base material. This increase is attributed to the precipitation hardening of Al_2Cu second phase;
- the joints welded at 100 mm/min and 1500 rpm achieved an ultimate tensile strength of approximately 335 MPa and an elongation at fracture of 8.5%. This represents only a 13% reduction in strength compared to the as-built condition, a smaller decrease than typically observed in friction stir welding of other additively manufactured alloys.

In summary, friction stir welding is a suitable method for welding additive manufacturing parts as it allows for the preservation of the engineering microstructure. Moreover, unlike fusion welding methods, defect control is much easier with this method. Therefore, friction stir welding is highly recommended for joining additive manufacturing components.

Acknowledgments

This study was supported by the interdepartmental research center on advanced joining technologies - J-Tech@PoliTO - of the Politecnico di Torino (http://www.j-tech.polito.it/).

This paper is recommended by the Hungarian Welding Society (MAHEG) and is the written extract of the conference presentation presented in the XXXII. International Welding Conference, Dunaújváros, Hungary.

References

[1] Avateffazeli, M., Shakil, S. I., Hadadzadeh, A., Shalchi-Amirkhiz, B., Pirgazi, H., Mohammadi, M., Haghshenas, M. "On microstructure and work hardening behavior of laser powder bed fused Al-Cu-Mg-Ag-TiB_2 and AlSi10Mg alloys", Materials Today Communication, 35, 105804, 2023. https://doi.org/10.1016/J.MTCOMM.2023.105804

[2] Kordijazi, A., Weiss, D., Das, S., Behera, S., Roshan, H. M., Rohatgi, P. "Effect of Solidification Time on Microstructure, Wettability, and Corrosion Properties of A205-T7 Aluminum Alloys", International Journal of Metalcasting, 15, pp. 2–12, 2021. https://doi.org/10.1007/S40962-020-00457-8

[3] Li, S., Cai, B., Duan, R., Tang, L., Song, Z., White, D., Magdysyuk, O. V., Attallah, M. M. "Synchrotron Characterisation of Ultra-Fine Grain TiB_2/Al-Cu Composite Fabricated by Laser Powder Bed Fusion", Acta Metallurgica Sinica (English Letters), 35, pp. 78–92, 2022. https://doi.org/10.1007/S40195-021-01317-y

[4] Avateffazeli, M., Shakil, S. I., Khan, M. F., Pirgazi, H., Shamsaei, N., Haghshenas, M. "The effect of heat treatment on fatigue response of laser powder bed fused Al-Cu-Mg-Ag-TiB_2 (A20X) alloy", Materials Today Communication, 35, 106009, 2023. https://doi.org/10.1016/J.MTCOMM.2023.106009

[5] Shakil, S. I., Zoeram, A. S., Pirgazi, H., Shalchi-Amirkhiz, B., Poorganji, B., Mohammadi, M., Haghshenas, M. "Microstructural-micromechanical correlation in an Al–Cu–Mg–Ag–TiB_2 (A205) alloy: additively manufactured and cast", Materials Science and Engineering: A, 832, 142453, 2022. https://doi.org/10.1016/J.MSEA.2021.142453

[6] Barode, J., Vayyala, A., Virgillito, E., Aversa, A., Mayer, J., Fino, P., Lombardi, M. "Revisiting heat treatments for additive manufactured parts: A case study of A20X alloy", Materials & Design, 225, 111566, 2023. https://doi.org/10.1016/J.MATDES.2022.111566

[7] Ghasri-Khouzani, M., Karimialavijeh, H., Pröbstle, M., Batmaz, R., Muhammad, W., Chakraborty, A., Sabiston, T. D., Harvey, J. P., Martin, É. "Processability and characterization of A20X aluminum alloy fabricated by laser powder bed fusion", Materials Today Communication, 35, 105555, 2023. https://doi.org/10.1016/J.MTCOMM.2023.105555

[8] Avateffazeli, M., Khan, M. F., Shamsaei, N., Haghshenas, M. "Microstructure, Mechanical, and Fatigue Properties of a Laser Powder Bed Fused Al-Cu-Mg-Ag-Ti-B (A205) Alloy", In: International Solid Freeform Fabrication Symposium: Proceedings of the 33rd Annual International Solid Freeform Fabrication Symposium – An Additive Manufacturing Conference, Texas, USA, 2022. https://doi.org/10.26153/TSW/44159

[9] Avateffazeli, M., Carrion, P. E., Shachi-Amirkhiz, B., Pirgazi, H., Mohammadi, M., Shamsaei, N., Haghshenas, M. "Correlation between tensile properties, microstructure, and processing routes of an Al–Cu–Mg–Ag–TiB_2 (A205) alloy: Additive manufacturing and casting", Materials Science and Engineering: A, 841, 142989, 2022. https://doi.org/10.1016/J.MSEA.2022.142989

[10] Shakil, S. I., Zoeram, A. S., Avateffazeli, M., Roscher, M., Pirgazi, H., Shalchi-Amirkhiz, B., Poorganji, B., Mohammadi, M., Haghshenas, M. "Ambient-temperature time-dependent deformation of cast and additive manufactured Al-Cu-Mg-Ag-TiB_2 (A205)", Micron, 156, 103246, 2022. https://doi.org/10.1016/J.MICRON.2022.103246

[11] Meyers, M. A., Chawla, K. K. "Mechanical Behavior of Materials", Cambridge University Press, 2008. ISBN: 9780511810947 https://doi.org/10.1017/CBO9780511810947

[12] ISO "ISO 6892-1:2016 Metallic materials – Tensile testing, Part 1: Method of test at room temperature", International Organization for Standardization, Geneva, Swizterland, 2016. [online] Available at: https://www.iso.org/standard/61856.html [Accessed: 31 March 2024]

[13] DIN "DIN 50125:2016-12 Testing of metallic materials - Tensile test pieces", Deutsches Institut für Normung, Berlin, Germany, 2016.

[14] ASTM "ASTM E92-17 Standard Test Methods for Vickers Hardness and Knoop Hardness of Metallic Materials", ASTM International, West Conshohocken, PA, USA, 2017. https://doi.org/10.1520/E0092-17

[15] Jamshidi Aval, H. "Effect of heat input in dissimilar friction stir welding of A390-10 wt.% SiC composite–AA2024 aluminum alloy", Archives of Civil and Mechanical Engineering, 24(3), 17, 2024. https://doi.org/10.1007/S43452-024-00957-Y

[16] Ahmed, M. M. Z., Ataya, S., El-Sayed Seleman, M. M., Mahdy, A. M. A., Alsaleh, N. A., Ahmed, E. "Heat Input and Mechanical Properties Investigation of Friction Stir Welded AA5083/AA5754 and AA5083/AA7020", Metals, 11(1), 68, 2021. https://doi.org/10.3390/MET11010068

[17] Akinlabi, E. T., Akinlabi S. A. "Effect of Heat Input on the Properties of Dissimilar Friction Stir Welds of Aluminium and Copper", American Journal of Materials Science, 2(5), pp. 147–152, 2012. https://doi.org/10.5923/J.MATERIALS.20120205.03

[18] Su, H., Wu, C. S., Pittner, A., Rethmeier, M. "Simultaneous measurement of tool torque, traverse force and axial force in friction stir welding", Journal of Manufacturing Processes, 15(4), pp. 495–500, 2013. https://doi.org/10.1016/J.JMAPRO.2013.09.001

[19] Rometsch, P. A., Zhu, Y., Wu, X., Huang, A. "Review of high-strength aluminum alloys for additive manufacturing by laser powder bed fusion", Materials & Design, 219, 110779, 2022. https://doi.org/10.1016/J.MATDES.2022.110779

[20] Ghoncheh, M. H., Sanjari, M., Zoeram, A. S., Cyr, E., Amirkhiz, B. S., Lloyd, A., Haghshenas, M., Mohammadi, M. "On the microstructure and solidification behavior of new generation additively manufactured Al-Cu-Mg-Ag-Ti-B alloys", Additive Manufacturing, 37, 101724, 2021. https://doi.org/10.1016/J.ADDMA.2020.101724

[21] Sauvage, X., Dédé, A., Muñoz, A. C., Huneau, B. "Precipitate stability and recrystallisation in the weld nuggets of friction stir welded Al-Mg-Si and Al-Mg-Sc alloys", Materials Science and Engineering: A, 491(1−2), pp. 364–371, 2008. https://doi.org/10.1016/J.MSEA.2008.02.006

[22] Moeini, G., Sajadifar, S. V., Wegener, T., Rössler, C., Gerber, A., Böhm, S., Niendorf, T. "On the influence of build orientation on properties of friction stir welded Al–Si10Mg parts produced by selective laser melting", Journal of Materials Research and Technology, 12, pp. 1446–1460, 2021. https://doi.org/10.1016/J.JMRT.2021.03.101

[23] Liu, G., Murr, L. E., Niou, C. S., McClure, J. C., Vega, F. R. "Microstructural aspects of the friction-stir welding of 6061-T6 aluminum", Scripta Materialia, 37(3), pp. 355–361, 1997. https://doi.org/10.1016/S1359-6462(97)00093-6

[24] Genevois, C., Deschamps, A., Denquin, A., Doisneau-Cottignies, B. "Quantitative investigation of precipitation and mechanical behaviour for AA2024 friction stir welds", Acta Materialia, 53(8), pp. 2447–2458, 2005. https://doi.org/10.1016/j.actamat.2005.02.007

[25] Dumont, M., Steuwer, A., Deschamps, A., Peel, M., Withers, P. J. "Microstructure mapping in friction stir welds of 7449 aluminium alloy using SAXS", Acta Materialia, 54(18), pp. 4793–4801, 2006. https://doi.org/10.1016/j.actamat.2006.06.015

[26] Fonda, R. W., Bingert, J. F. "Precipitation and grain refinement in a 2195 Al friction stir weld", Metallurgical and Materials Transactions A, 37(12), pp. 3593–3604, 2006. https://doi.org/10.1007/s11661-006-1054-2

[27] Schneider, J. A., Nunes, A. C., Chen, P. S., Steele, G. "TEM study of the FSW nugget in AA2195-T81", Journal of Materials Science, 40(16), pp. 4341–4345, 2005. https://doi.org/10.1007/s10853-005-2808-8

[28] Du, Z., Tan, M. J., Chen, H., Bi, G., Chua, C. K. "Joining of 3D-printed AlSi10Mg by friction stir welding", Welding in the World, 62(3), pp. 675–682, 2018. https://doi.org/10.1007/S40194-018-0585-7

[29] Moeini, G., Sajadifar, S. V., Wegener, T., Brenne, F., Niendorf, T., Böhm, S. "On the low-cycle fatigue behavior of friction stir welded Al–Si12 parts produced by selective laser melting", Materials Science and Engineering: A, 764, 138189, 2019. https://doi.org/10.1016/J.MSEA.2019.138189